Geosci. Model Dev. Discuss., https://doi.org/10.5194/gmd-2018-336
Manuscript under review for journal Geosci. Model Dev.
Discussion started: 1 April 2019

Geoscientific Model Development Discussions

Toward an open-access of high-frequency lake modelling and statistics data for scientists and practitioners. The case of Swiss Lakes using Simstrat v2.1

Adrien Gaudard[1†], Love Råman Vinnå[1], Fabian Bärenbold[1], Martin Schmid[1], Damien Bouffard[1]

[1]Surface Waters Research and Management, Eawag, Swiss Federal Institute of Aquatic Sciences and Technology, Kastanienbaum, Switzerland
[†] deceased, 2019

Correspondence to: Damien Bouffard (damien.bouffard@eawag.ch)

Abstract

One-dimensional hydrodynamic lake models are nowadays widely recognized as key tools. They offer the possibility to study processes at high frequency, here referring to hourly time scale, to analyse scenarios and test hypothesizes. Yet, simulation outputs are mainly used by the modellers themselves and often not easily reachable for the outside community. We have developed an openly accessible web-based platform for visualization and promotion of easy access to lake model output data updated in near real time (simstrat.eawag.ch). This platform was developed for 54 lakes in Switzerland with potential for adaptation to other regional areas or even at global worldwide scale using appropriate forcing input data. The benefit of this data platform is here practically illustrated with two examples. First we show that the output data allows for assessing the long term effects of past climate change on the thermal structure of a lake. In the second case, we demonstrate how the data platform can be used to study and compare the role of episodic strong wind events for different lakes on a regional scale and especially how they temporary destabilize their thermal structure. With this open access data platform we demonstrate the path forward for scientists and practitioners promoting a cross-exchange of expertise through openly sharing of in-situ and model data.

Geosci. Model Dev. Discuss., https://doi.org/10.5194/gmd-2018-336
Manuscript under review for journal Geosci. Model Dev.
Discussion started: 1 April 2019

1 Introduction

Aquatic research is particularly oriented towards providing relevant tools and expertise for practitioners. Understanding and monitoring inland waters is most often based on *in situ* observations. Today, the physical and biogeochemical properties of many lakes are monitored using monthly to bi-monthly vertical discrete profiles. Yet, part of the dynamics is not captured at this temporal scale (Kiefer et al., 2015). An emerging alternative approach consists in deploying long-term moorings with sensors and loggers at different depths of the water column. However, this approach is scarcely used for monitoring purposes at the country-scale, although it is promoted by research initiatives such as GLEON (Hamilton et al., 2015) or NETLAKE (Jennings et al., 2017).

It is common to parameterize aquatic physical processes with mechanistic models, and ultimately use them to understand aquatic systems through scenario investigation or climate projection. In the last decades, many lake models have been developed. Although never perfect, they have been shown to reproduce very well the thermal structure of natural lakes (Bruce et al., 2018). Today's most widely referenced one-dimensional (1D) models include (alphabetic order) DYRESM (Antenucci and Imerito, 2000), FLake (Mironov, 2005), GLM (Hipsey et al., 2014), GOTM (Burchard et al., 1999), LAKE (Stepanenko et al., 2016), Minlake (Riley and Stefan, 1988), MyLake (Saloranta and Andersen, 2007), and Simstrat (Goudsmit et al., 2002). Unfortunately, the results from these models are mainly used by the modellers themselves, and often not easily accessible for the outside community.

The performance of lake models is determined by the physical representativeness of the algorithms and by the quality of the input data. The latter include (i) lake morphology, (ii) atmospheric forcing, (iii) hydrological cycle (e.g. inflow, outflow and/or water level fluctuations), and (iv) light absorption. *In situ* observations (e.g., temperature profiles) are often used for calibration of model parameters, which remains a time-consuming process. To be successful, such an endeavour requires observations of a broad, representative range of conditions in the system. To support this approach, it is important to promote and facilitate the sharing of existing datasets of observations among scientists and practitioners. Conversely, scientists and practitioners should benefit from the model output, which is often ready-to-use, high-frequency and up-to-date. Yet, model output data should not only be seen as a toolbox for temporal interpolation. It also provides properties that are helpful for specific analyses but difficult to measure (e.g., the heat content to assess the global impact of climate change, or the vertical diffusivity to estimate vertical turbulent transport), and it can support the interpretation of biogeochemical observations, if the relevant processes are driven by thermal stratification and mixing. In a global context of open science, collaboration between the different actors and reuse of field and model output data should be fostered. Such win-win collaboration serves the interests of lake modellers, researchers, field scientists, lake managers, lake users, and more generally the public.

In this work, we present a new and improved version of the Simstrat lake model. This version is applied as part of a multi-lake modelling project with the intention of making our extensive results openly accessible. We present the deployment of a fully

automated workflow, which simulates the thermal structure of lakes in Switzerland and weekly updates an online platform (https://simstrat.eawag.ch) with metadata, plots and results.

2 Methods

2.1 Model and workflow

We use the 1D lake model Simstrat v2.1 to model 54 Swiss lakes or basins (see Appendix A for details of modelled lakes) in an automated way. Simstrat was first introduced by Goudsmit et al. (2002) and has been successfully applied to a number of lakes (Gaudard et al., 2017; Perroud et al., 2009; Råman Vinnå et al., 2018; Schwefel et al., 2016; Thiery et al., 2014). Recently, large parts of the code were refactored using the object-oriented Fortran 2003 standard. This version of Simstrat allows for a clearer, modular code structure. The source code of Simstrat v2.1 is openly available via GitHub at: https://github.com/Eawag-AppliedSystemAnalysis/Simstrat/releases/tag/v2.1. In addition to refactoring, a simpler build procedure was implemented using a docker container. This portable build environment contains all necessary software dependencies for the build process of Simstrat. It can thereby be used on both Windows and Linux systems. A step-by-step guide is provided on GitHub.

In addition to the improvements already described by Schmid and Köster (2016), Simstrat v2.1 includes (i) the possibility to use gravity-driven inflow and a wind drag coefficient varying with wind speed – both described by Gaudard et al. (2017), and (ii) an ice and snow module. The ice and snow module employed is based on the work of Leppäranta (2014, 2010) and Saloranta and Andersen (2007), and is further described in Appendix B.

A Python script was developed to (i) retrieve the newest forcing data directly from data providers and integrate them into the existing datasets, (ii) process the input data and prepare the full model and calibration setups, (iii) run calibration of the model for chosen model parameters, (iv) provide output results, and (v) update an online platform to display these results. The script is controlled by an input file written in JSON format, which specifies the lakes to be modelled together with their physical properties (depth, volume, bathymetry, etc.) and identifies the meteorological and hydrological stations to be used for model forcing. The overall workflow is illustrated in Figure 1.

2.2 Input data

Table 1 summarizes the type and sources of the data fed to Simstrat. For meteorological forcing, homogenized hourly data from Federal Office of Meteorology and Climatology (MeteoSwiss, CH) weather stations are used. For each lake the most relevant weather stations are used. Air temperature is corrected for the small altitude difference between the lake and the meteorological station, assuming an adiabatic vertical rate of -0.0065 °C m^{-1}. For hydrological forcing, homogenized hourly data from the stations operated by the Federal Office for the Environment (FOEN) are used. For each lake, the data from the available stations at the inflows are aggregated to feed the model with a single inflow. The aggregated discharge is the sum of the discharge of all the inflows, and the aggregated temperature is the weighted average of the inflows for which temperature

is measured. Inflows are disabled if no discharge or temperature data is available at all. The light absorption coefficient $\varepsilon_{\mathrm{abs}}$ [m^{-1}] is either obtained from Secchi depth z_{Secchi} [m] measurements, or is set to a constant value based on the lake trophic status. In the first case, the following equation is applied: $\varepsilon_{\mathrm{abs}} = 1.7/z_{\mathrm{Secchi}}$ (Poole and Atkins, 1929). In the second case, $\varepsilon_{\mathrm{abs}}$ is set to 0.15 m^{-1} for oligotrophic lakes, 0.25 m^{-1} for mesotrophic lakes, and 0.50 m^{-1} for eutrophic lakes. For glacier-fed lakes (typical above 2000 m) rich in sedimentary material, $\varepsilon_{\mathrm{abs}}$ is set to 1.00 m^{-1}.

Missing forcing data within that timeframe can cause significant discrepancies in the model and needs to be properly handled. We apply different simple data patching methods depending on the data and the number of missing data. For all variables, gaps of less than one day are completed by linear interpolation. For highly seasonal variables (air temperature, solar radiation, humidity, inflow discharge, inflow temperature, light absorption), missing data are replaced by the corresponding day-of-year averages obtained from the available data. For cloud coverage, missing data are obtained as one minus the ratio between measured solar radiation and 90 % of the theoretical solar radiation. The latter is calculated as described in Appendix C.

The timeframe of the model is determined by the availability of the necessary meteorological data (air temperature, solar radiation, humidity, wind, precipitation). Initial conditions for temperature and salinity are set using conductivity-temperature-depth (CTD) profiles.

2.3 Calibration

Model parameters are set to logical default values, and four of them are calibrated (see Table 2). The parameters to calibrate were selected according to their importance for the model (e.g. based on previous sensitivity analysis). The number of parameters is deliberately kept small in order to maintain the calibration process simple and focused. Calibration is performed using PEST v15.0 (see http://pesthomepage.org), a model-independent parameter estimation software (Doherty, 2016). As a reference for calibration, temperature observations from CTD profiles are used. Calibration is performed on a yearly basis, unless significant changes are made to either the model, the forcing data, or the observational data. For the eight lakes to which no observations are available, parameters are set to their default value (see Table 2) with no calibration preformed, and the lack of calibration is clearly indicated on the online platform.

2.4 Output

From the model results, we directly obtain time series of several model output variables (in particular temperature, salinity, Brunt-Väisälä frequency, vertical diffusivity, and ice thickness). In addition, we use the following known physical and lake-related properties: the acceleration of gravity $g = 9.81$ m^2 s^{-1}, the heat capacity of water $c_{\mathrm{p}} = 4.18 \cdot 10^3$ J K^{-1} kg^{-1} the volume of the lake V [m^3], the area A_z [m^2], temperature T_z [K], and density ρ_z [kg m^{-3}] at depth z [m], and the mean lake depth $\bar{z} = \frac{1}{V}\int z\ A_z\ dz$ [m]. From this, we calculate time series of derived values:

- Mean lake temperature: $\bar{T} = \frac{1}{V}\int T_z\, A_z\, dz$ [K]

- Heat content: $H = c_p \int \rho_z \, T_z \, A_z \, dz$ [J]
- Schmidt stability: $S_T = \frac{g}{A_0} \int (z - \bar{z}) \, \rho_z \, A_z \, dz$ [J m^{-2}]
- Timing of summer stratification: we use a threshold based on the Schmidt stability to determine beginning and end of summer stratification. The lake is assumed to be stratified for $S_T / z_{lake} \geq 10$ J m^{-3}. Using a different criterion (e.g., temperature difference between surface and bottom water) results in variations in the calculated stratification period; however, the general pattern among lakes remains similar).
- Timing of ice cover: we use the existence of ice to determine beginning and end of ice covered period.

From these results, we create static and interactive plots. The latter are created using the Plotly Python Library (see https://plot.ly/python). The plots can be categorized as follows:

- History (e.g., contour plot of the whole temperature time series, line plot of the whole time series of Schmidt stability);
- Current situation (e.g., latest temperature profile);
- Statistics (e.g., average monthly temperature profiles, long-term trends).

An online platform (accessible at https://simstrat.eawag.ch) is automatically weekly fed with model results, metadata and plots for all the 54 modelled lakes (see Figure 2). Such a platform allows for efficient display and sharing of the model results for interested users, and is built for straightforward application to other lakes outside Switzerland.

3 Results and discussion

Model output data is very well-suited for comparison analyses, and studies of long-term change. The Simstrat model provides regional long-term high-frequency data updated in near real-time as output. This represents a novel way to monitor, analyse and visualize processes in aquatic systems, and, most importantly, grant the entire community direct access to the findings. The coupling between Simstrat and PEST provides an effective way to calibrate model parameters automatically. The uncertainty quantification finally allows an appropriate informed use of the output data. Yet, more advanced methods for both parameter estimation and uncertainty quantification such as Bayesian inference (Gelman et al., 2013) should be interfaced to Simstrat. Similarly, the simple data patching applied for missing input data would benefit from state of the art data science methods in the future.

Out of the 46 calibrated lakes, the post-calibration root mean square error (RMSE) is < 1 °C for 17 lakes, between 1 and 1.5 °C for 15 lakes, between 1.5 and 2 °C for 8 lakes and > 2 °C for 6 lakes (Figure 3). This is comparable to the RMSE range of ~0.7-2.1 °C reported in a recent 32-lake modelling study using GLM (Bruce et al., 2018).

We illustrate the potential of high-frequency lake model data with two examples: first by briefly showing the long-term changes caused by climate change in Lake Brienz (section 3.1), and secondly by investigating the differential response of lakes across Switzerland to episodic forcing (short-term extremes, section 3.2).

Geosci. Model Dev. Discuss., https://doi.org/10.5194/gmd-2018-336
Manuscript under review for journal Geosci. Model Dev.
Discussion started: 1 April 2019

3.1 Long-term evolution of the thermal structure of lakes, response to climate trends.

Lake Brienz (https://simstrat.eawag.ch/LakeBrienz, Figure 2) situated in central Switzerland at 564 m asl is a typical deep (259 m) oligotrophic peri-alpine lake with a retention time of 2.6 years (Wüest et al., 2007). The effect of the upstream hydropower operation were previously shown to shift riverine particle inputs from summer to winter in this lake (Finger et al., 2006, 2007). Changes in the lake thermal structure from modifications of riverine particle inputs and discharge regime in a context of climate warming was recently quantified for nearby Lake Biel and Lake Geneva (Råman Vinnå et al., 2018).

Over the period 1981–2015, we observe an increase in both yearly averaged surface and bottom temperatures with significant ($p<0.001$) trends of +0.64 °C/decade and +0.11 °C/decade respectively (Figure 4a). Analysis from in situ observation for the same period indicates a trend for the surface temperature around 0.72 °C/decade ($p\sim0.07$). This is in line with epilimnion/hypolimnion trends observed in neighbouring deep lakes ranging from +0.22/+0.11 °C/decade in Lake Geneva (Lemmin and Amouroux, 2006) to +0.41/+0.13 °C/decade in Lower Lake Zürich (Schmid and Köster, 2016; Livingstone, 2003). The vertical heterogeneous heating observed in Lake Brienz is also consistent with previous observations showing that difference in warming between the surface and the bottom increase the strength and length of the stratified period (Zhong et al., 2016; Wahl and Peeters, 2014). We detect an earlier onset of the stratification in spring of -7.5 day/decade ($p<0.001$) and a later breakdown of the stratification by +3.7 day/decade ($p<0.001$) (Figure 4c). Both the warming trend and the increase in length of the stratified period increase the Schmid stability (Figure 4e) and heat content (Figure 4f). The increase of Lake Brienz heat content amounts to $\sim2\cdot10^{16}$ J over 38 years, which corresponds to roughly two thirds of the heat extraction potential for this lake (Gaudard et al., 2019). Contrarily to the above-described variables, no clear trend was detectable in the yearly maximum stratification strength (Brunt-Väisälä frequency, Figure 4d).

The observed increase in overall stability (Figures 4e and 4e) reduces vertical mixing and affects the vertical storage of heat with less heat transferred immediately below the thermocline (Figure 4b) with a slight decrease in temperature observed in autumn at ~30 m depth. Additionally, this effect is clearly seen in Lake Geneva (Figure 5, https://simstrat.eawag.ch/LakeGeneva) with the surface waters warming strongly (+1 °C/decade in June), resulting in a cooling layer between 20 and 60 m (-0.2 °C/decade) in late summer. Such reduction of vertical exchange is self-strengthening and enhances the vertical differential warming.

Similar analysis was repeated for all the modelled lakes: an inter-comparison of the temporal extent of both summer and winter stratification is illustrated in Figure 6. An altitude-dependent decrease of the duration of summer stratification is observed, along with a stronger corresponding increase in the duration of the inverse winter stratification from 1200 m asl. This is possibly linked to an altitude dependency of climate-driven warming in Swiss lakes, first reported by Livingstone et al. (2005), caused by a delay in meltwater runoff (Sadro et al., 2018). Here this process is not directly resolved but incorporated through the calibration procedure spanning all seasons.

Geosci. Model Dev. Discuss., https://doi.org/10.5194/gmd-2018-336
Manuscript under review for journal Geosci. Model Dev.
Discussion started: 1 April 2019

3.2 Event based evolution of the lake thermal structure.

A major drawback of traditional lake monitoring programs in Switzerland is the coarse temporal resolution, with measurements often performed on a monthly basis. Thought sufficient for direct long-term trend studies when conducted over long period typically longer than 30 years (Gray et al., 2018), traditional monitoring programs cannot resolve the impact of short-term events and their consequences for the ecosystem. This is however a strength of high-frequency (hourly time scale) lake modelling, which allows for simulation and comparison of the effects associated with rapid and often brutal events such as storms. Based on high-frequency observations, Woolway et al. (2018) showed the effects of a major storm on Lake Windermere. They observed a decrease in the strength of the stratification, a deepening of the thermocline and the onset of internal waves oscillations ultimately upwelling oxygen depleted cold water into the downstream river. Furthermore, Perga et al. (2018) illustrated how storms could be just as important as gradual long-term trends for changes in light penetration and thermal structure in an Alpine lake.

Here we demonstrate how high-frequency model output can be used to study the influence of specific events on the thermal dynamics of lakes. As an example, we focus on the 28th of June 2018 when Switzerland experienced a strong but by no means exceptional storm with Northern winds mainly affecting the North-Western part of the country – the mean wind speed during that day is shown spatially in Figure 7a. The evolution of the stratification strength, illustrated here by the Schmidt stability, is given in Figure 7b for one of the most affected lakes, Lake Neuchâtel (https://simstrat.eawag.ch/LakeNeuchatel, Figure 2). This lake, with the main axis well-aligned to synoptical winds, experienced a ~8 % decrease in the Schmidt stability over this half-day event. Yet, the effects were not long-lasting and the Schmidt stability reverted to its pre-storm value within ~5 days (Figure 7b). This also resulted in a total increase of the lake heat content by ~$1.4 \cdot 10^{16}$ J from the start of the storm to the time of recovery. We used the Schmidt stability recovery duration as a way to assess the short-term effect of the storm on the different modelled lakes. In Figure 7a, lakes are coloured based on the delay in Schmidt stability increase (in days) caused by the storm. The impact of the storm was obviously not limited to Lake Neuchâtel but rather showed a regionally-varying pattern. Particularly small- to medium-sized lakes in the North-Western parts of Switzerland were more affected than large lakes or lakes located in the Southern part of Switzerland. However, the thermal structure of the lakes quickly reverted to the seasonal spring warming trend.

So far, climate-driven warming has been recognized to cause an overall increase in lake stratification strength and duration, and a gradual warming of the different layers (Schwefel et al., 2016; Zhong et al., 2016; Wahl and Peeters, 2014). Air temperature trend was the most studied forcing parameter. Yet, the dynamics of extreme events (such as heat waves, drought spells, storms), including their changes in strength and distribution, has been comparatively overlooked. Scenario exploration, climate change studies, or historical forcing reanalysis should be integrated in such web-based hydrodynamic platforms to assess their roles in modifying the lake thermal structures and heat storage.

4 Conclusion

The workflow presented in this paper allows sharing of high-frequency, up-to-date and permanently available lake model results for multiple users and purposes. These results are well suited for the following applications and target groups:

- For the public, the platform serves as an informative website enabling easy access to broad quantities of regional scientific results, with the intention of raising interest about lake ecosystem dynamics.
- For lake managers, the platform makes relevant information, such as (i) current temperature and stratification conditions of the lakes, (ii) simple statistical analyses such as monthly temperature profiles and long-term temperature trends.
- For researchers, this work can facilitate (i) scenario modelling of any of the lakes, as the basic model setup is ready-to-use, (ii) improvement of the lake model with addition of previously unresolved processes (e.g., ice cover and river intrusion), (iii) access to variables that were previously not or irregularly available (e.g., vertical diffusivity, heat content, stratification and heat fluxes), and (iv) specific comparative analyses, whereby a given question can be investigated simultaneously over many lakes (e.g., the impact of climate change).

Code and data availability

The workflow was developed for Swiss lakes but can be easily extended to other geographical area or at global scale by using other meteorological input data. Simstrat and the Python workflow are available on https://github.com/Eawag-AppliedSystemAnalysis/Simstrat/releases/tag/v2.1 (https://doi.org/10.5281/zenodo.2600709) and https://github.com/Eawag-AppliedSystemAnalysis/Simstrat-WorkflowModellingSwissLakes (https://doi.org/10.5281/zenodo.2607153).

Author contribution

The new version of Simstrat was developed by FB. The workflow was developed by AG. The ice model was developed by LVR. The concept of the workflow was defined by DB. All authors contributed to the validation of the model and interpretation of the results. AG and DB wrote the manuscript with contributions from FB, LVR and MS.

Competing interests

The authors declare that they have no conflict of interest

Acknowledgment

We thank Davide Vanzo for helping with the Docker and the scripts and Michael Pantic for helping restructuring the version 2.1 of Simstrat. We finally thank Marie-Elodie Perga for her comments on a preliminary version of the manuscript. The full list of acknowledgement regarding in-situ observations can be found here: https://simstrat.eawag.ch/impressum .

References

Antenucci, J. and Imerito, A.: The CWR dynamic reservoir simulation model DYRESM, Science Manual, The University of Western Australia, Perth, Australia., 2000.

Bruce, L. C., Frassl, M. A., Arhonditsis, G. B., Gal, G., Hamilton, D. P., Hanson, P. C., Hetherington, A. L., Melack, J. M., Read, J. S., Rinke, K., Rigosi, A., Trolle, D., Winslow, L., Adrian, R., Ayala, A. I., Bocaniov, S. A., Boehrer, B., Boon, C., Brookes, J. D., Bueche, T., Busch, B. D., Copetti, D., Cortés, A., de Eyto, E., Elliott, J. A., Gallina, N., Gilboa, Y., Guyennon, N., Huang, L., Kerimoglu, O., Lenters, J. D., MacIntyre, S., Makler-Pick, V., McBride, C. G., Moreira, S., Özkundakci, D., Pilotti, M., Rueda, F. J., Rusak, J. A., Samal, N. R., Schmid, M., Shatwell, T., Snorthheim, C., Soulignac, F., Valerio, G., van der Linden, L., Vetter, M., Vinçon-Leite, B., Wang, J., Weber, M., Wickramaratne, C., Woolway, R. I., Yao, H. and Hipsey, M. R.: A multi-lake comparative analysis of the General Lake Model (GLM): Stress-testing across a global observatory network, Environmental Modelling & Software, 102, 274–291, doi:10.1016/j.envsoft.2017.11.016, 2018.

Burchard, H., Bolding, K. and Villarreal, M. R.: GOTM, a general ocean turbulence model: theory, implementation and test cases, Space Applications Institute., 1999.

Doherty, J.: PEST: Model-Independent Parameter Estimation, 6th ed., Watermark Numerical Computing, Australia., 2016.

Finger, D., Schmid, M. and Wüest, A.: Effects of upstream hydropower operation on riverine particle transport and turbidity in downstream lakes, Water Resources Research, 42(8), doi:10.1029/2005WR004751, 2006.

Finger, D., Bossard, P., Schmid, M., Jaun, L., Müller, B., Steiner, D., Schäffer, E., Zeh, M. and Wüest, A.: Effects of alpine hydropower operations on primary production in a downstream lake, Aquat. Sci., 69(2), 240–256, doi:10.1007/s00027-007-0873-6, 2007.

Gaudard, A., Schwefel, R., Råman Vinnå, L., Schmid, M., Wüest, A. and Bouffard, D.: Optimizing the parameterization of deep mixing and internal seiches in one-dimensional hydrodynamic models: A case study with Simstrat v1.3, Geosci. Model Dev., 10(9), 3411–3423, doi:10.5194/gmd-10-3411-2017, 2017.

Gaudard, A., Wüest, A. and Schmid, M.: Using lakes and rivers for extraction and disposal of heat: Estimate of regional potentials, Renewable Energy, 134, 330–342, doi:10.1016/j.renene.2018.10.095, 2019.

Gelman, A., Carlin, J., Stern, H. and Rubin, D.: Bayesian Data Analysis, 3rd ed., Chapman and Hall/CRC, New York., 2013.

Gill, A. E.: Atmosphere-Ocean Dynamics, Academic Press, San Diego, California, USA. [online] Available from: http://books.google.ch/books?hl=de&lr=&id=8kFPh_SvnAIC&oi=fnd&pg=PP2&dq=Atmosphere-Ocean+dynamics&ots=B77L2z3Shp&sig=6rVJ55ftAUHkMDEC_NzBEgkL2Lw (Accessed 31 January 2014), 1982.

Goudsmit, G.-H., Burchard, H., Peeters, F. and Wüest, A.: Application of k-ϵ turbulence models to enclosed basins: The role of internal seiches, Journal of Geophysical Research: Oceans, 107(C12), 3230, doi:10.1029/2001JC000954, 2002.

Gray, D. K., Hampton, S. E., O'Reilly, C. M., Sharma, S. and Cohen, R. S.: How do data collection and processing methods impact the accuracy of long-term trend estimation in lake surface-water temperatures?, Limnology and Oceanography: Methods, 16(8), 504–515, doi:10.1002/lom3.10262, 2018.

Hamilton, D. P., Carey, C. C., Arvola, L., Arzberger, P., Brewer, C., Cole, J. J., Gaiser, E., Hanson, P. C., Ibelings, B. W., Jennings, E., Kratz, T. K., Lin, F.-P., McBride, C. G., Marques, M. D. de, Muraoka, K., Nishri, A., Qin, B., Read, J. S., Rose, K. C., Ryder, E., Weathers, K. C., Zhu, G., Trolle, D. and Brookes, J. D.: A Global Lake Ecological Observatory Network

(GLEON) for synthesising high-frequency sensor data for validation of deterministic ecological models, Inland Waters, 5(1), 49–56, doi:10.5268/IW-5.1.566, 2015.

Hipsey, M. R., Bruce, L. C. and Hamilton, D. P.: GLM - General Lake Model. Model overview and user information, Technical Manual, The University of Western Australia, Perth, Australia. [online] Available from: http://swan.science.uwa.edu.au/downloads/AED_GLM_v2_0b0_20141025.pdf, 2014.

Jennings, E., Eyto, E., Laas, A., Pierson, D., Mircheva, G., Naumoski, A., Clarke, A., Healy, M., Šumberová, K. and Langenhaun, D.: The NETLAKE Metadatabase—A Tool to Support Automatic Monitoring on Lakes in Europe and Beyond, Limnology and Oceanography Bulletin, 26(4), 95–100, doi:10.1002/lob.10210, 2017.

Kiefer, I., Odermatt, D., Anneville, O., Wüest, A. and Bouffard, D.: Application of remote sensing for the optimization of in-situ sampling for monitoring of phytoplankton abundance in a large lake, Sci. Total Environ., 527–528, 493–506, doi:10.1016/j.scitotenv.2015.05.011, 2015.

Lemmin, U. and Amouroux, A.: The influence of climate change on Lake Geneva, SIL Proceedings, 1922-2010, 29(4), 1806–1810, doi:10.1080/03680770.2006.11903000, 2006.

Leppäranta, M.: Modelling the Formation and Decay of Lake Ice, in The Impact of Climate Change on European Lakes, edited by G. George, pp. 63–83, Springer Netherlands, Dordrecht., 2010.

Leppäranta, M.: Freezing of lakes and the evolution of their ice cover, Springer, New York., 2014.

Livingstone, D. M.: Impact of secular climate change on the thermal structure of a large temperate central European lake, Climatic change, 57(1–2), 205–225, 2003.

Livingstone, D. M., Lotter, A. F. and Kettle, H.: Altitude-dependent differences in the primary physical response of mountain lakes to climatic forcing, Limnology and Oceanography, 50(4), 1313–1325, 2005.

Meyers, T. P. and Dale, R. F.: Predicting Daily Insolation with Hourly Cloud Height and Coverage, J. Climate Appl. Meteor., 22(4), 537–545, doi:10.1175/1520-0450(1983)022<0537:PDIWHC>2.0.CO;2, 1983.

Mironov, D. V.: Parameterization of lakes in numerical weather prediction. Part 1: Description of a lake model, German Weather Service, Offenbach am Main, Germany., 2005.

Perga, M.-E., Bruel, R., Rodriguez, L., Guénand, Y. and Bouffard, D.: Storm impacts on alpine lakes: Antecedent weather conditions matter more than the event intensity, Glob Chang Biol, 24(10), 5004–5016, doi:10.1111/gcb.14384, 2018a.

Perroud, M., Goyette, S., Martynov, A., Beniston, M. and Anneville, O.: Simulation of multiannual thermal profiles in deep Lake Geneva: A comparison of one-dimensional lake models, Limnology and Oceanography, 54(5), 1574–1594, 2009.

Poole, H. H. and Atkins, W. R. G.: Photo-electric measurements of submarine illumination throughout the year, Journal of the Marine Biological Association of the United Kingdom, 16(1), 297–324, 1929.

Råman Vinnå, L., Wüest, A., Zappa, M., Fink, G. and Bouffard, D.: Tributaries affect the thermal response of lakes to climate change, Hydrol. Earth Syst. Sci., 22(1), 31–51, doi:10.5194/hess-22-31-2018, 2018.

Riley, M. J. and Stefan, H. G.: Minlake: A dynamic lake water quality simulation model, Ecological Modelling, 43(3), 155–182, doi:10.1016/0304-3800(88)90002-6, 1988.

Sadro, S., Sickman, J. O., Melack, J. M. and Skeen, K.: Effects of Climate Variability on Snowmelt and Implications for Organic Matter in a High-Elevation Lake, Water Resources Research, 54(7), 4563–4578, doi:10.1029/2017WR022163, 2018.

Saloranta, T. M.: Modeling the evolution of snow, snow ice and ice in the Baltic Sea, Tellus A, 52(1), 93–108, doi:10.1034/j.1600-0870.2000.520107.x, 2000.

Saloranta, T. M. and Andersen, T.: MyLake—A multi-year lake simulation model code suitable for uncertainty and sensitivity analysis simulations, Ecological Modelling, 207(1), 45–60, 2007.

Schmid, M. and Köster, O.: Excess warming of a Central European lake driven by solar brightening, Water Resour. Res., 52(10), 8103–8116, doi:10.1002/2016WR018651, 2016.

Schwefel, R., Gaudard, A., Wüest, A. and Bouffard, D.: Effects of climate change on deep-water oxygen and winter mixing in a deep lake (Lake Geneva)–Comparing observational findings and modeling, Water Resources Research, 52(11), 8811–8826, doi:10.1002/2016WR019194, 2016.

Smith, W. L.: Note on the Relationship Between Total Precipitable Water and Surface Dew Point, J. Appl. Meteor., 5(5), 726–727, doi:10.1175/1520-0450(1966)005<0726:NOTRBT>2.0.CO;2, 1966.

Stepanenko, V. M., Mammarella, I., Ojala, A., Miettinen, H., Lykosov, V. and Vesala, T.: LAKE 2.0: a model for temperature, methane, carbon dioxide and oxygen dynamics in lakes, Geosci. Model Dev., 9(5), 1977–2006, doi:10.5194/gmd-9-1977-2016, 2016.

Thiery, W., Stepanenko, V. M., Fang, X., Jöhnk, K. D., Li, Z., Martynov, A., Perroud, M., Subin, Z. M., Darchambeau, F., Mironov, D. V. and others: LakeMIP Kivu: evaluating the representation of a large, deep tropical lake by a set of one-dimensional lake models, Tellus A: Dynamic Meteorology and Oceanography, 66(1), 21390, doi:10.3402/tellusa.v66.21390, 2014.

Wahl, B. and Peeters, F.: Effect of climatic changes on stratification and deep-water renewal in Lake Constance assessed by sensitivity studies with a 3D hydrodynamic model, Limnology and Oceanography, 59(3), 1035–1052, doi:10.4319/lo.2014.59.3.1035, 2014.

Woolway, R. I., Simpson, J. H., Spiby, D., Feuchtmayr, H., Powell, B. and Maberly, S. C.: Physical and chemical impacts of a major storm on a temperate lake: a taste of things to come?, Climatic Change, 151(2), 333–347, doi:10.1007/s10584-018-2302-3, 2018.

Wüest, A., Zeh, M. and Ackerman, J. D.: Lake Brienz Project: An interdisciplinary catchment-to-lake study, Aquat. Sci., 69(2), 173–178, doi:10.1007/s00027-007-0016-0, 2007.

Yen, Y. C.: Review of thermal properties of snow, ice and sea ice, Cold Regions Research and Engineering Laboratory, Hanover, New Hampshire., 1981.

Zhong, Y., Notaro, M., Vavrus, S. J. and Foster, M. J.: Recent accelerated warming of the Laurentian Great Lakes: Physical drivers, Limnology and Oceanography, 61, 1762–1786, doi:10.1002/lno.10331, 2016.

Geosci. Model Dev. Discuss., https://doi.org/10.5194/gmd-2018-336
Manuscript under review for journal Geosci. Model Dev.
Discussion started: 1 April 2019

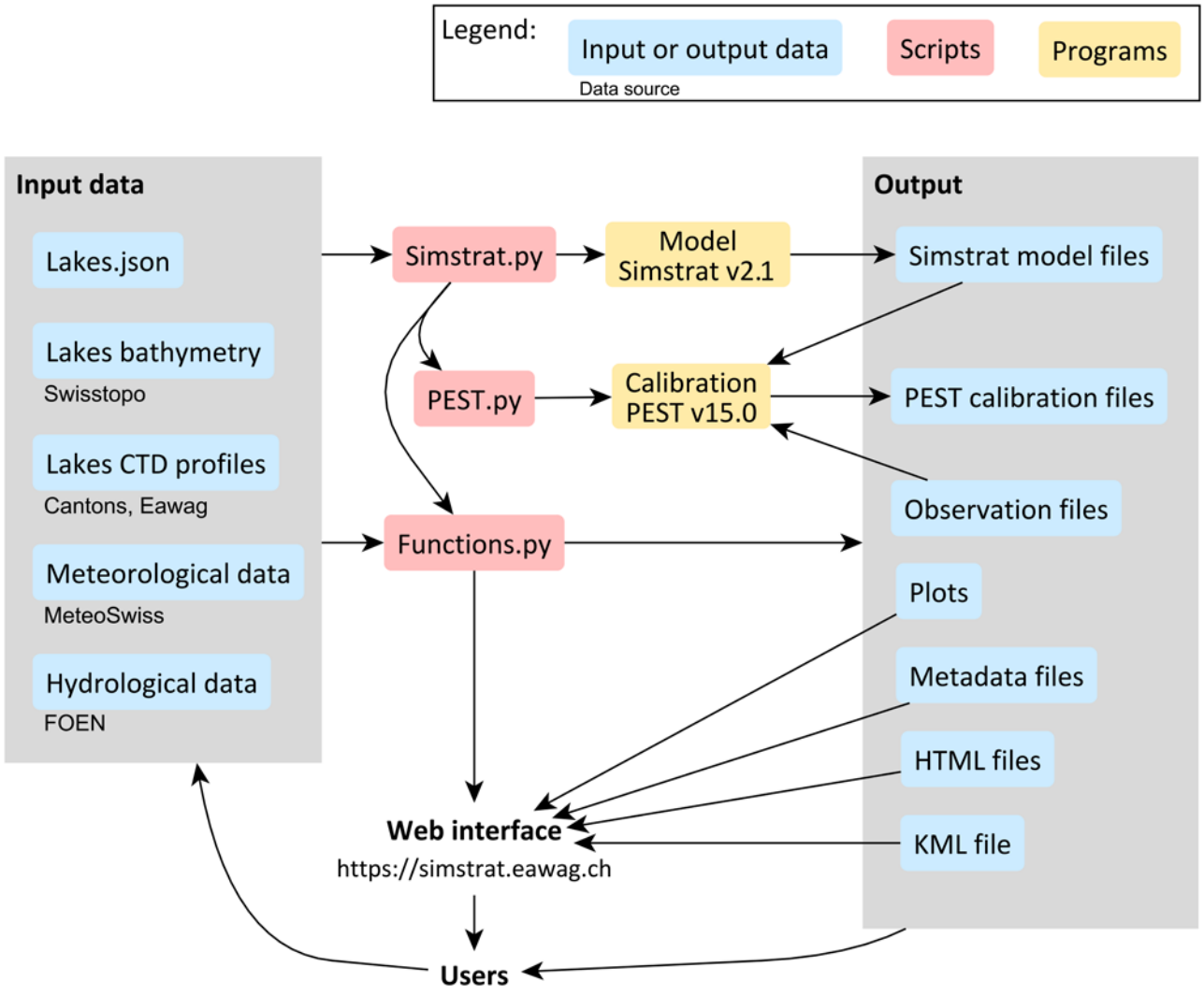

Figure 1. General workflow diagram. Model input data (left box) is retrieved and processed by the Python script "Simstrat.py", which runs the model (Simstrat v2.0) and/or model calibration (using PEST v15.0) and produces output (right box). This output is then uploaded to a web interface (https://simstrat.eawag.ch) for general use. All scripts and programs are available on https://github.com/Eawag-AppliedSystemAnalysis/Simstrat/releases/tag/v2.1 and https://github.com/Eawag-AppliedSystemAnalysis/Simstrat-WorkflowModellingSwissLakes .

Geosci. Model Dev. Discuss., https://doi.org/10.5194/gmd-2018-336
Manuscript under review for journal Geosci. Model Dev.
Discussion started: 1 April 2019

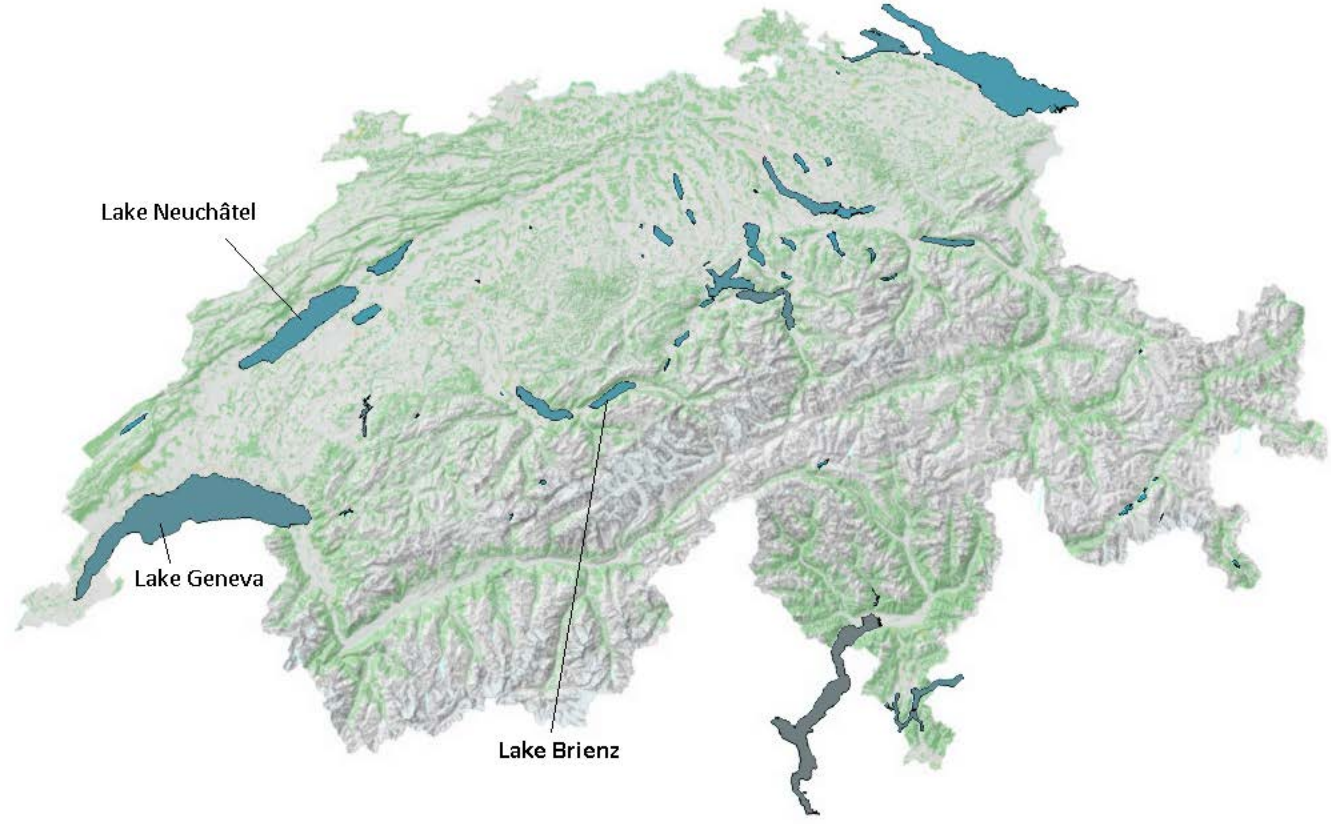

Figure 2. Snapshop of the interactive map displayed on the homepage of the online platform: https://simstrat.eawag.ch. Status on December 4th, 2018 (3D view). The location of the lakes discussed in this manuscript is also indicated.

Geosci. Model Dev. Discuss., https://doi.org/10.5194/gmd-2018-336
Manuscript under review for journal Geosci. Model Dev.
Discussion started: 1 April 2019

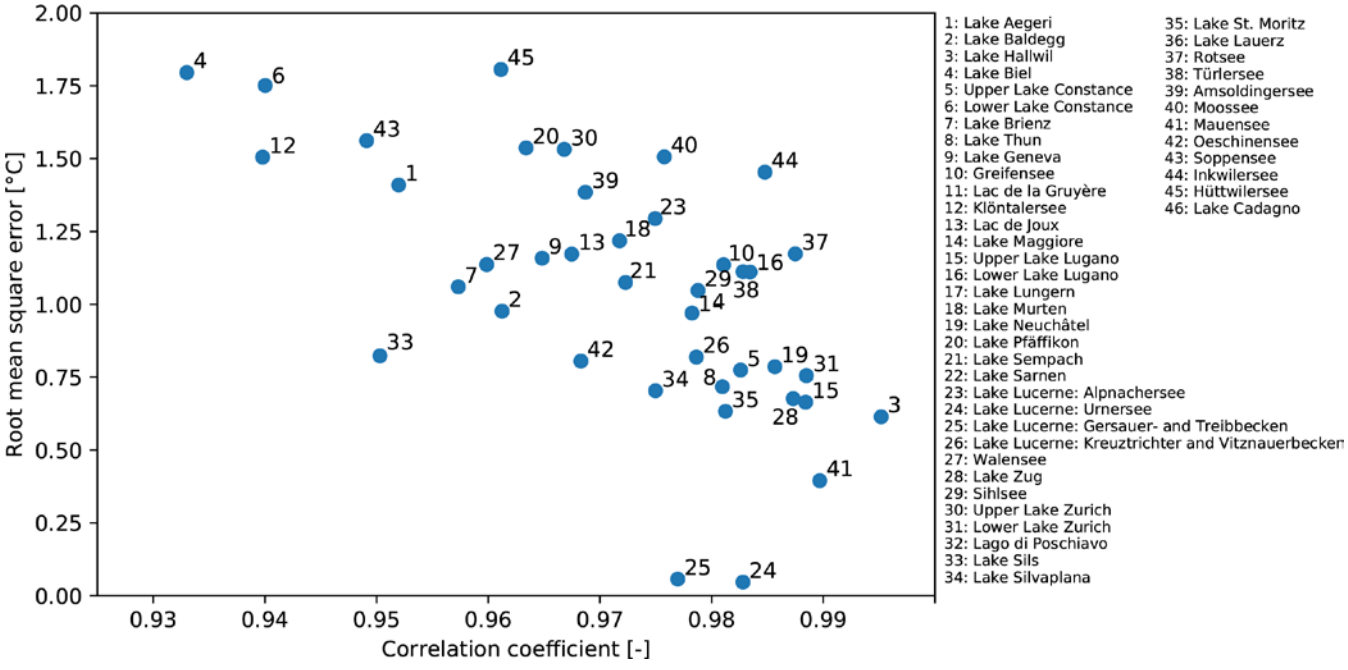

Figure 3. Performance of the model for the different lakes, as shown by the root mean square error (RMSE) and the correlation coefficient. Six lakes with RMSE > 2 °C are not shown.

Geosci. Model Dev. Discuss., https://doi.org/10.5194/gmd-2018-336
Manuscript under review for journal Geosci. Model Dev.
Discussion started: 1 April 2019

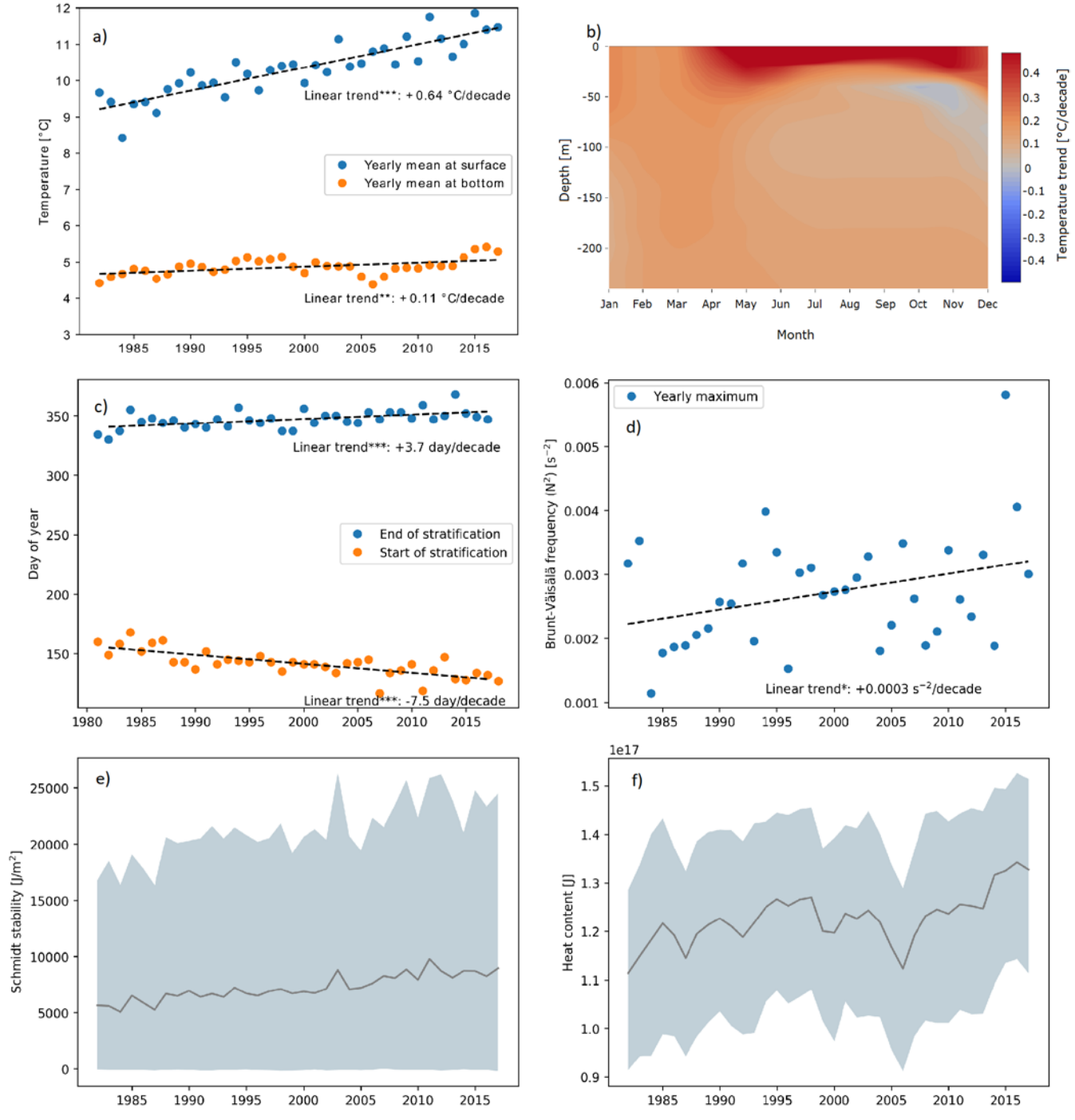

Figure 4. Evolution of several indicators for Lake Brienz over the period 1981-2018: (a) yearly mean surface and bottom temperatures, with linear regression, (b) contour plot of the linear temperature trend through depth and month, (c) yearly start and end day of summer stratification, with linear regression, (d) yearly maximum Brunt-Väisälä frequency, with linear regression,

Geosci. Model Dev. Discuss., https://doi.org/10.5194/gmd-2018-336
Manuscript under review for journal Geosci. Model Dev.
Discussion started: 1 April 2019

Geoscientific Model Development Discussions

(e) yearly mean (line), min and max (shaded area) Schmidt stability, (f) yearly mean (line), min and max (shaded area) heat content. The asterisks indicate the p-value of the linear trend: * for p<0.001, ** for p<0.01, and * for p<0.05.**

Geosci. Model Dev. Discuss., https://doi.org/10.5194/gmd-2018-336
Manuscript under review for journal Geosci. Model Dev.
Discussion started: 1 April 2019

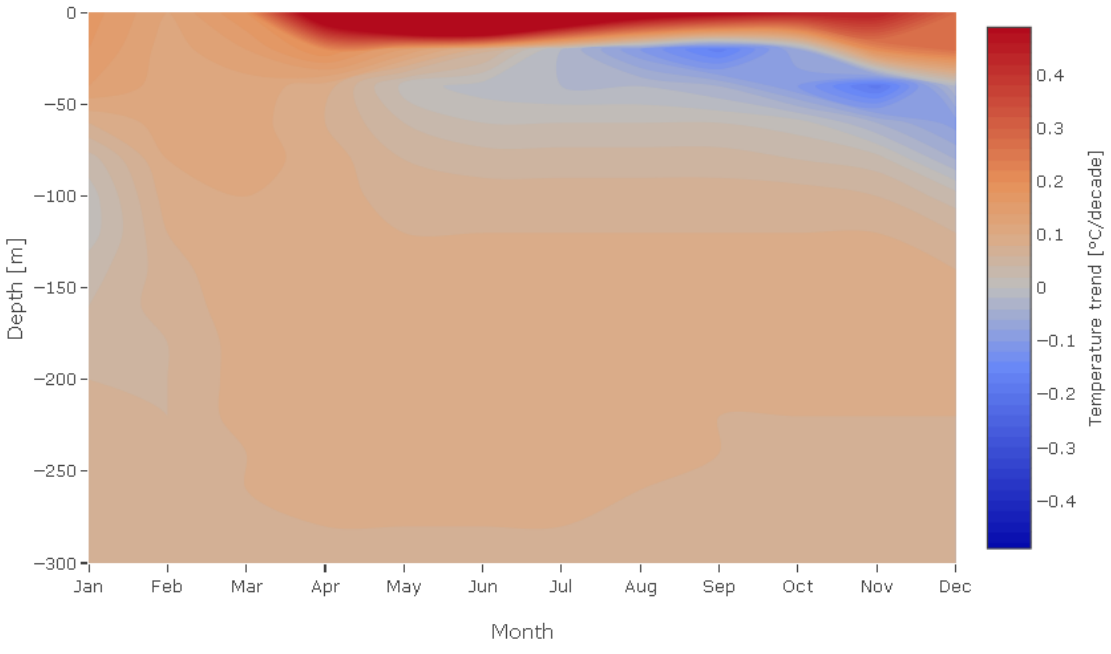

Figure 5. Vertical and seasonal temperature trends modelled in Lake Geneva over the period 1981-2018. Values are given on a monthly basis.

Geosci. Model Dev. Discuss., https://doi.org/10.5194/gmd-2018-336
Manuscript under review for journal Geosci. Model Dev.
Discussion started: 1 April 2019

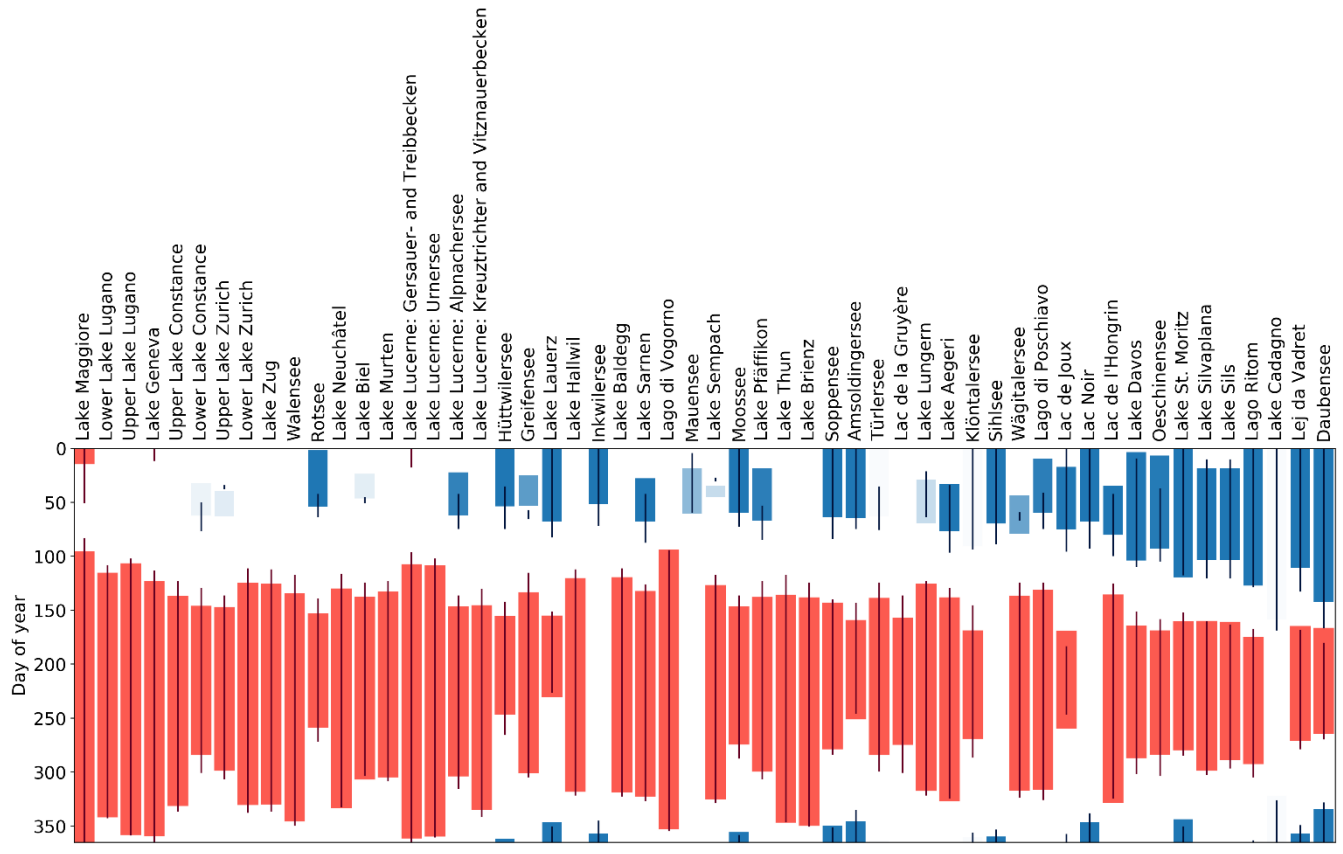

Figure 6. Comparison of timing of stratification and ice cover for the considered lakes. The coloured areas represent the mean periods of summer stratification (red) and ice cover (blue); the vertical lines represent the last year (here, 2017). The transparency for the ice cover indicates the freezing frequency: full transparency means that ice was never modelled, while no transparency means that ice was modelled every winter. Lakes are ordered from left to right based on elevation.

Geosci. Model Dev. Discuss., https://doi.org/10.5194/gmd-2018-336
Manuscript under review for journal Geosci. Model Dev.
Discussion started: 1 April 2019

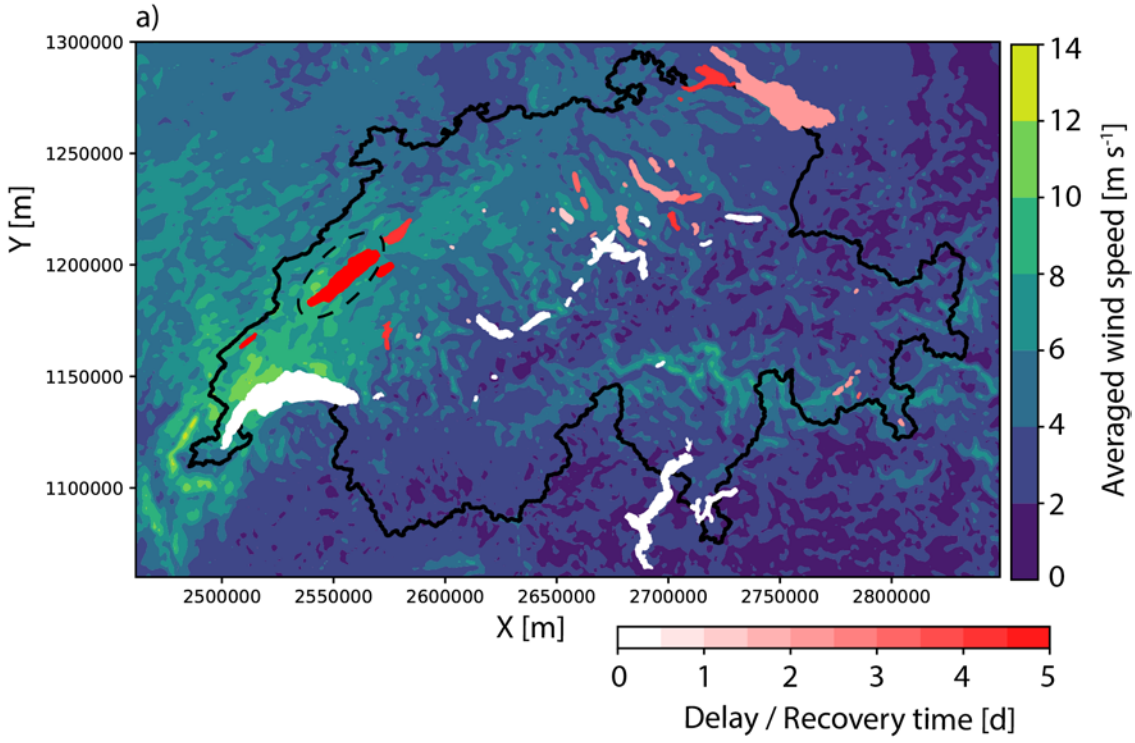

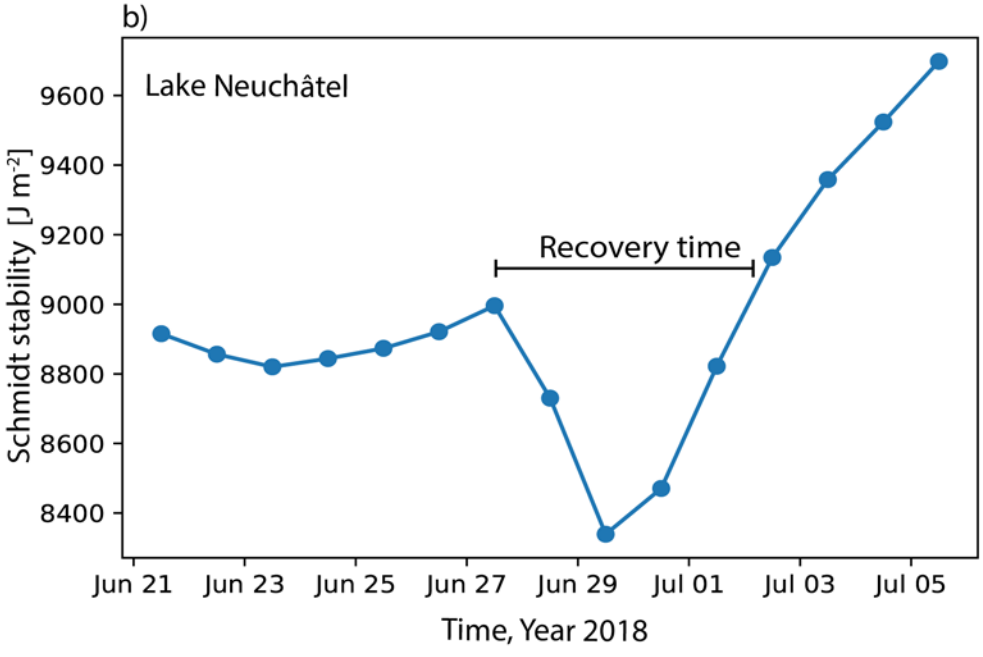

Geosci. Model Dev. Discuss., https://doi.org/10.5194/gmd-2018-336
Manuscript under review for journal Geosci. Model Dev.
Discussion started: 1 April 2019

Geoscientific Model Development Discussions

Figure 7. (a) Mean wind field on June 28th, 2018 (data source: MeteoSwiss, COSMO-1 model, coordinate system CH1903+) and delay in Schmidt stability increase for the modelled lakes: from no delay (white) to a delay of more than 5 days (red). (b) Schmidt stability (daily average) in Lake Neuchâtel during the period of the storm.

Geosci. Model Dev. Discuss., https://doi.org/10.5194/gmd-2018-336
Manuscript under review for journal Geosci. Model Dev.
Discussion started: 1 April 2019

Table 1. Input data sources used for the model

Data	Source	Model input
Lake bathymetry	Swisstopo (https://www.swisstopo.admin.ch)	Bathymetry profile
Meteorological forcing	MeteoSwiss (http://meteoswiss.admin.ch)	Air temperature, solar radiation, humidity, wind, cloud cover, precipitation
Hydrological forcing	FOEN (http://hydrodaten.admin.ch)	Inflow discharge, inflow temperature
Secchi depth	Eawag, cantonal monitoring	Light absorption coefficient
CTD profiles	Eawag, cantonal monitoring	Initial conditions, temperature observations for calibration

Geosci. Model Dev. Discuss., https://doi.org/10.5194/gmd-2018-336
Manuscript under review for journal Geosci. Model Dev.
Discussion started: 1 April 2019

Geoscientific Model Development Discussions

Table 2. Model parameters. The asterisk (*) indicates the parameters that were calibrated. The geothermal heat flux is based on existing geothermal data for Switzerland: https://www.geocat.ch/geonetwork/srv/eng/md.viewer#/full_view/2d8174b2-8c4a-44ea-b470-cb3f216b90d1.

Parameter	Description and units	Default value
lat	Latitude [°]	Based on lake location
p_air	Air pressure [mbar]	Based on lake elevation
a_seiche*	Ratio of wind energy going into seiche energy [-]	Based on lake size
q_nn	Fractionation coefficient for seiche energy [-]	1.10
f_wind*	Scaling factor for wind speed [-]	1.00
c10	Scaling factor for the wind drag coefficient [-]	1.00
cd	Bottom drag coefficient [-]	0.002
hgeo	Geothermal heat flux [W/m^2]	Based on geothermal map (see table caption)
p_radin*	Scaling factor for the incoming long wave radiation [-]	1.00
p_windf	Scaling factor for the fluxes of sensible and latent heat [-]	1.00
albsw	Albedo of water for short wave radiation [-]	0.09
beta_sol	Fraction of short wave radiation absorbed as heat in the uppermost water layer [-]	0.35
p_albedo*	Scaling factor for snow/ice albedo, thereby affecting melting and under ice warming [-]	1.00
freez_temp	Water freezing temperature [°C]	0.01
snow_temp	Temperature below which precipitation falls as snow [°C]	2.00

Geosci. Model Dev. Discuss., https://doi.org/10.5194/gmd-2018-336
Manuscript under review for journal Geosci. Model Dev.
Discussion started: 1 April 2019

Appendix

A. Properties of the modelled lakes

The following table summarizes the main properties of the 54 lakes we model in this work. The full dataset is available as a JSON file. An asterisk after the lake name indicates that this lake was not calibrated due to the lack of observational data.

Lake	Volume [km^3]	Surface [km^2]	Max depth [m]	Elevation [m]	Weather station IDs (MeteoSwiss)	Hydrological station IDs (FOEN)	Model timeframe
Lake Aegeri	0.36	7.3	83	724	AEG, SAG, EIN	-	2012-2018
Lake Baldegg	0.174	5.2	66	463	MOA	-	2012-2018
Lake Hallwil	0.285	10.3	48	449	MOA	2416	2012-2018
Lake Biel	1.12	39.3	74	429	CRM	2085, 2307, 2446	1993-2018
Upper Lake Constance	47.6	473	251	395	ARH, GUT	2473, 2308, 2312	1981-2018
Lower Lake Constance	0.8	63	45	395	STK, HAI, GUT	-	1981-2018
Lake Brienz	5.17	29.8	259	564	INT	2019, 2109	1981-2018
Lake Thun	6.5	48.3	217	558	THU, INT	2457, 2469, 2488	1981-2018
Lake Geneva	89	580	309	372	PUY	2009, 2432, 2433, 2486, 2493	1981-2018
Greifensee	0.15	8.5	32	435	SMA	-	1981-2018
Lac de la Gruyère	0.22	9.6	75	677	MAS, GRA	2160, 2412	2011-2018
Klöntalersee	0.056	3.3	45	848	GLA	-	1981-2018
Lac de Joux	0.145	8.77	32	1004	CHB, BIE	-	2009-2018
Lago di Vogorno*	0.1	1.68	204	470	OTL	2605	1981-2018
Lake Maggiore	37	212	372	193	OTL	2068, 2368	1981-2018
Upper Lake Lugano	4.69	27.5	288	271	LUG	2321	1981-2018
Lower Lake Lugano	1.14	20.3	95	271	LUG	2629, 2461	1981-2018

Lake Lungern	0.065	2	68	688	GIH	-	2010-2018
Lake Murten	0.55	22.8	45	429	NEU	2034	1981-2018
Lake Neuchâtel	13.8	218	152	429	NEU	2378, 2369, 2480, 2458, 2447	1981-2018
Lake Pfäffikon	0.059	3.3	36	537	SMA	-	1981-2018
Lake Sempach	0.66	14.5	87	504	EGO	2608	2010-2018
Lake Sarnen	0.239	7.5	51	469	GIH	-	2010-2018
Lake Lucerne: Alpnachersee	0.1	4.5	35	434	LUZ	2102, 2436	1981-2018
Lake Lucerne: Urnersee	3.16	22	200	434	ALT	2056, 2276	1981-2018
Lake Lucerne: Gersauer- and Treibbecken	4.41	30	214	434	GES, ALT	2084, 2481	1981-2018
Lake Lucerne: Kreuztrichter and Vitznauerbecken	4.35	59	151	434	LUZ	-	1981-2018
Walensee	2.5	24.2	151	419	QUI, LAC, GLA	2372, 2426	1981-2018
Lake Zug	3.2	38.3	197	417	CHZ, WAE	2477	1981-2018
Sihlsee	0.096	11.3	22	889	EIN	2300, 2635	2012-2018
Wägitalersee*	0.15	4.18	65	900	LAC, EIN	-	2012-2018
Upper Lake Zurich	0.47	20.3	48	406	WAE	2104	1981-2018
Lower Lake Zurich	3.36	68.2	136	406	LAC, SCM, WAE	-	1981-2018
Lago di Poschiavo	0.12	1.98	85	962	ROB	2078	1981-2018
Lake Sils	0.137	4.1	71	1797	SIA	-	2014-2018
Lake Silvaplana	0.14	2.7	77	1791	SIA	-	2014-2018

Lake St. Moritz	0.02	0.78	44	1768	SAM	2105	1981-2018
Lake Lauerz	0.0234	3.07	14	447	GES, LUZ	-	1981-2018
Rotsee	0.00381	0.48	16	419	LUZ	-	1981-2018
Daubensee*		0.64	50	2207	BLA	-	2013-2018
Lej da Vadret*		0.43	50	2160	SIA	-	2014-2018
Lake Davos*	0.0156	0.59	54	1558	DAV	-	1981-2018
Lac de l'Hongrin*	0.0532	1.6	105	1250	CHD	-	2012-2018
Türlersee	0.00649	0.497	22	643	WAE	-	1981-2018
Amsoldingersee	0.00255	0.382	14	641	THU	-	2012-2018
Lac Noir*	0.00252	0.47	10	1045	PLF	-	1989-2018
Moossee	0.00339	0.31	21	521	BER	-	1981-2018
Mauensee		0.55	9	504	EGO	-	2010-2018
Oeschinensee	0.0402	1.11	56	1578	ABO	-	1983-2018
Soppensee	0.00286	0.25	27	596	EGO	-	2010-2018
Inkwilersee	0.00094	0.102	6	461	KOP	-	2011-2018
Hüttwilersee		0.34	28	434	HAI	-	2010-2018
Lake Cadagno	0.00242	0.26	21	1921	PIO	-	1981-2018
Lago Ritom*	0.048	1.49	69	1850	PIO	-	1981-2018

Geosci. Model Dev. Discuss., https://doi.org/10.5194/gmd-2018-336
Manuscript under review for journal Geosci. Model Dev.
Discussion started: 1 April 2019

B. Ice module

The ice and snow module employed is based on the work of Leppäranta (2014, 2010) and Saloranta and Andersen (2007), and includes the following physical processes:

- Air temperature dependent formation and growth of black ice, including the insulating effect of a snow cover.
- Snow layer build-up, including the compression effect due to the weight of fresh snow.
- Buoyancy-driven formation of white ice.
- Short wave irradiance reflection and penetration into the underlying water column.
- Melting of snow, white and black ice due to both the direct heat flux through the atmospheric interface and the absorption of short wave irradiance.

Three layers are used to represent black ice, white ice, and snow. An instant supply of water through cracks in the black ice is assumed to occur in order to form white ice. The water stored in ice and snow is neither withdrawn during ice formation nor added during melting to the water balance. Furthermore, the effect of liquid water pools on top of or between the layers is neglected

Below the freezing point (ice formation)

The ice module is activated as the water temperature in the topmost grid cell T_w (°C) drops below the freezing temperature T_f (°C). T_f can be set to zero for a vertical grid size ≤ 0.5 m, the user can adapt (raise) this value to fit coarser grids. If temperature is below the freezing point, the energy incorporated into the change of state E_f is calculated as

$$E_f = \rho_w c_{pw} z_1 (T_f - T_w) \quad \text{(B1)}$$

here ρ_w (1000 kg m^{-3}) is the density of fresh water, c_{pw} the heat capacity of water (4182 J kg^{-1} °C^{-1}) and z_1 the height of the topmost grid cell. E_f and the latent heat of freezing l_h ($3.34 \cdot 10^5$ J kg^{-1}) as well as the density of black ice ρ_{ib} (916.2 kg m^{-3}) are used for calculating the initial height of black ice h_{ib} (m) in Eq. B2, thereafter T_w is set equal to T_f

$$h_{ib} = E_f / (l_h \rho_{ib}) \quad \text{(B2)}$$

If an ice cover is present and if the atmospheric temperature T_a (°C) is smaller or equal to T_f, the growth of black ice dh_{ib}/dt continues as described in (Saloranta and Andersen, 2007).

$$\frac{dh_{ib}}{dt} = \sqrt{2k_i / (\rho_{ib} * l_h) * (T_f - T_i)} \quad \text{(B3)}$$

Here k_i (2.22 W K^{-1} m^{-1}) is the thermal conductivity of ice at 0 °C and T_i (°C) the ice temperature calculated as

Geosci. Model Dev. Discuss., https://doi.org/10.5194/gmd-2018-336
Manuscript under review for journal Geosci. Model Dev.
Discussion started: 1 April 2019

$$T_i = \frac{PT_f + T_a}{1+P} \tag{B4}$$

$$P = \max\left(\frac{k_i h_s}{k_s h_{ib}}, \frac{1}{10 h_{ib}}\right) \tag{B5}$$

There k_s (0.2 W K^{-1} m^{-1}) is the thermal conductivity of snow and h_s (m) the height of the snow layer. When T_a is smaller than the snow temperature (default set to 2 °C) water equivalent precipitation p_r (m hour^{-1}) is turned into fresh snow h_{s_new} (m) as

$$h_{s\_new} = p_r \frac{\rho_w}{\rho_{s0}} \tag{B6}$$

where ρ_{s0} (250 kg m^{-3}) is the initial snow density. The existing snow cover h_s (m) undergoes compression (first terms Eq. B7 and B8) by the new layer as described in Yen (1981), thereafter the new and existing layers are combined in both height and density (second terms of Eqs. B7 and B8).

$$\frac{dh_s}{dt} = -h_s\left(1 - \frac{\rho_s}{[\rho_s + d\rho_s]}\right) + h_{s\_new} \tag{B7}$$

$$\frac{d\rho_s}{dt} = \rho_s C_1 w_s e^{-C_2\rho_s} - \left(\rho_s - \frac{\rho_s h_s + \rho_{s0} h_{s\_new}}{h_s + h_{s\_new}}\right) \tag{B8}$$

here ρ_s (kg m^{-3}) is the snow layer density kept within $\rho_{s0} < \rho_s < \rho_{sm}$ with the maximum snow density set to 450 kg m^{-3}, C_1 (5.8 m^{-1} hour^{-1}) and C_2 (0.021 m^3 kg^{-1}) are snow compression constants, and w_s (m) is the total weight above the layer under compression expressed in water equivalent height.

If the snow mass m_s (kg m^{-2}) becomes heavier than the upward acting buoyancy force B_i (kg m^{-2}), white ice with height h_{iw} (m) and density ρ_{iw} (875 kg m^{-3} Saloranta, 2000) is formed between the snow and the black ice layers to achieve equilibrium between B_i and m_s.

$$B_i = h_{ib}\left(\rho_w - \rho_{ib}\right) + h_{iw}\left(\rho_w - \rho_{iw}\right) \tag{B9}$$

$$\frac{dh_{iw}}{dt} = \frac{m_s - B_i}{\rho_s} \tag{B10}$$

Geosci. Model Dev. Discuss., https://doi.org/10.5194/gmd-2018-336
Manuscript under review for journal Geosci. Model Dev.
Discussion started: 1 April 2019

In this model, we assume continuous supply of water through cracks in the black ice to form white ice. The formation of white ice takes place instantaneously each time step and we do not consider the influence of pools under the snow for melting or short wave irradiance penetration.

Above the freezing point (melting)

If an ice cover is present and if $T_a > T_f$ melting starts. Each layer melts from above through the atmospheric interface and by penetrating short wave radiation

$$\frac{dh_{x\_upper}}{dt} = -\frac{H_{x\_y}}{(l_h + l_e)\rho_x} \tag{B11}$$

where H_{x_y} (W m^{-2}) is the layer-dependent heat flux (in the following, $_x$ represents $_s$, $_{iw}$ or $_{ib}$). The model supports melting through both sublimation (solid to gas) and non-sublimation (solid to liquid) with the inclusion/exclusion of the latent heat of evaporation l_e (J kg^{-1}). Non-sublimation melting is default with l_e set to zero, for sublimation melting the user can set l_e to 2265 kJ kg^{-1}. For the uppermost layer ($_y$ = $_{top}$, Eq. B12) the heat flux includes layer dependent uptake of short wave radiation H_{s_x}, long wave absorption H_a or layer dependent emission H_{w_x} as well as sensible H_k and latent H_v heat. If the layer is not in direct contact with the atmosphere, only H_s is used for melting from above ($_y$ = $_{under}$, Eq. B13).

$$H_{x\_top} = H_{s\_x} + H_a + H_{w\_x} + H_k + H_v \tag{B12}$$

$$H_{x\_under} = H_{s\_x} \tag{B13}$$

Here we follow Leppäranta (2014, 2010) for determining the heat flux terms in Eq. B12. The transmittance of short wave irradiance through each layer depends on each layers thickness h_x as well as on the layer specific bulk attenuation coefficient λ_x (m^{-1}; default λ_s = 24, λ_{iw} = 3 and λ_{ib} = 2; Leppäranta, 2014).

$$H_{s\_s} = I_s A_p (1 - A_x)\left(1 - e^{(-\lambda_s h_s)}\right) \tag{B14}$$

$$H_{s\_iw} = I_s A_p (1 - A_x)\left(e^{(-\lambda_s h_s)} - e^{(-\lambda_s h_s - \lambda_{iw} h_{iw})}\right) \tag{B15}$$

$$H_{s\_ib} = I_s A_p (1 - A_x)\left(e^{(-\lambda_s h_s - \lambda_{iw} h_{iw})} - e^{(-\lambda_s h_s - \lambda_{iw} h_{iw} - \lambda_{ib} h_{ib})}\right) \tag{B16}$$

Geosci. Model Dev. Discuss., https://doi.org/10.5194/gmd-2018-336
Manuscript under review for journal Geosci. Model Dev.
Discussion started: 1 April 2019

$$H_{s\_w} = I_s A_p (1 - A_x)\left(1 - e^{(-\lambda_s h_s - \lambda_{iw} h_{iw} - \lambda_{ib} h_{ib})}\right) \quad \text{(B17)}$$

There H_{s_w} is the radiation penetrating through the ice cover to the water below and I_s (W m^{-2}) the incoming short wave irradiance. We introduce the albedo parameter A_p which tunes short wave irradiance in order to match observed water temperatures, thus adjusting the melting and indirectly the duration of the ice cover. Furthermore, depending on which layer is in contact with the atmosphere we use a layer dependent constant albedo A_x (default A_s = 0.7, A_{iw} = 0.4 and A_{ib} = 0.3; Leppäranta, 2014).

$$A_x \begin{cases} A_s, h_s > 0 \\ A_{iw}, h_s = 0 \,\&\, h_{iw} > 0 \\ A_{ib}, h_s + h_{iw} = 0 \end{cases} \quad \text{(B18)}$$

Calculating H_a requires the long wave emission parameters k_a = 0.68, k_b = 0.036 (mbar^{-1}) and k_c = 0.18 (Leppäranta, 2010), atmospheric water vapour pressure e_a (mbar), cloud cover C and Stefan Boltzmann's constant σ (5.67*10^{-8} W m^{-2} K^{-4}). For Eqs. B19 and B20 the temperature T_x is given in Kelvin. H_{w_x} is layer dependent for the emissivity E_x with E_{iw} = E_{ib} = 0.97 and $E_s(\rho_s)$ from 0.8 at ρ_s = 250 kg m^{-3} to E_s = 0.9 for ρ_s = 450 kg m^{-3}. Calculating H_k and H_v requires the atmospheric density ρ_a = 1.2 kg m^{-3}, the heat capacity of air c_{pa} = 1005 J kg^{-1} K^{-1}, the wind speed at 10 m height w_{10}, the convective (b_c) and latent (b_l) bulk exchange coefficients both set to 0.0015 (Leppäranta, 2010; Gill, 1982), as well as the specific humidity both measured q_a (mbar) and at saturation q_0. There $q_a = 0.622 e_a / p_a$ where p_a is the air pressure and q_0 = 0.622*6.11/p_a at T_a= 0 °C (Leppäranta, 2014).

$$H_a = \left(k_a + k_b \sqrt{e_a}\left[1 + k_c C^2\right]\right)\sigma T_a^4 \quad \text{(B19)}$$

$$H_{w\_x} = E_x \sigma {T_f}^4 \quad \text{(B20)}$$

$$H_k = \rho_a c_{pa} b_c \left(T_a - T_f\right) w_{10} \quad \text{(B21)}$$

$$H_v = \rho_a l_h b_l \left(q_a - q_0\right) w_{10} \quad \text{(B22)}$$

As H_{s_w} warms the water under the ice, melting takes place from underneath with the energy H_{bottom} (W m^{-2}).

$$H_{bottom} = \left(T_w - T_f\right) c_{pw} \rho_w z_1 \quad \text{(B23)}$$

Geosci. Model Dev. Discuss., https://doi.org/10.5194/gmd-2018-336
Manuscript under review for journal Geosci. Model Dev.
Discussion started: 1 April 2019

After obtaining H_{bottom} the temperature of the first cell is set to T_f and the decrease of ice cover from below becomes

$$\frac{dh_{x\_lower}}{dt} = -\frac{H_{bottom}}{l_m \rho_x} \tag{B24}$$

Eq. B24 is only applied to h_{ib} and h_{iw}. In principle, h_s melts completely from above using Eq. B11 before h_{ib} and h_{iw} reach zero, however, if no ice is present, h_s is set to zero. By combining Eqs. B11 and B24 the total melting of each ice layer is calculated as

$$\frac{dh_x}{dt} = \frac{dh_{x\_lower}}{dt} + \frac{dh_{x\_upper}}{dt} \tag{B25}$$

When $h_x < 0$ due to melting the surplus energy is used for melting neighbouring layers according to the following procedure: if the melting is initiated from above the surplus energy is used to melt the layer directly underneath; if the melting is caused by the water below the layer directly above receives the surplus melting energy; if $h_{ib} <= h_{iw} <= 0$ the water in the topmost grid cell is heated with the remaining energy.

Ice model performance

To test the ice module, Simstrat was calibrated in Sihlsee with PEST using monthly resolved vertical temperature profiles (2006 to 2008, RMSE 1.2 °C) for four parameters including the new p_albedo parameter for scaling snow/ice albedo. Modelled and monthly measured total ice cover from 2012 to 2018 is shown in Fig. B1 (RMSE 0.078 m). The modelled thickness agrees well with measurements during years with an extensive ice covered period (2013, 2014 and 2017, max height > 5 cm). The model performance is not ideal for years with short temporal ice duration and thin ice thickness (2016 and 2018, max height < 5 cm). During these years, the quality of the forcing dataset becomes crucial. In the case of Sihlsee, the timing and duration of snowfall prolongs the duration of the ice-covered period. We use the meteorological station at Samedan (SAM) located four kilometres from the lake in a region with rapid topographical change. This in combination with monthly ice thickness measurements result in the divergence during 2016 and 2018.

Geosci. Model Dev. Discuss., https://doi.org/10.5194/gmd-2018-336
Manuscript under review for journal Geosci. Model Dev.
Discussion started: 1 April 2019

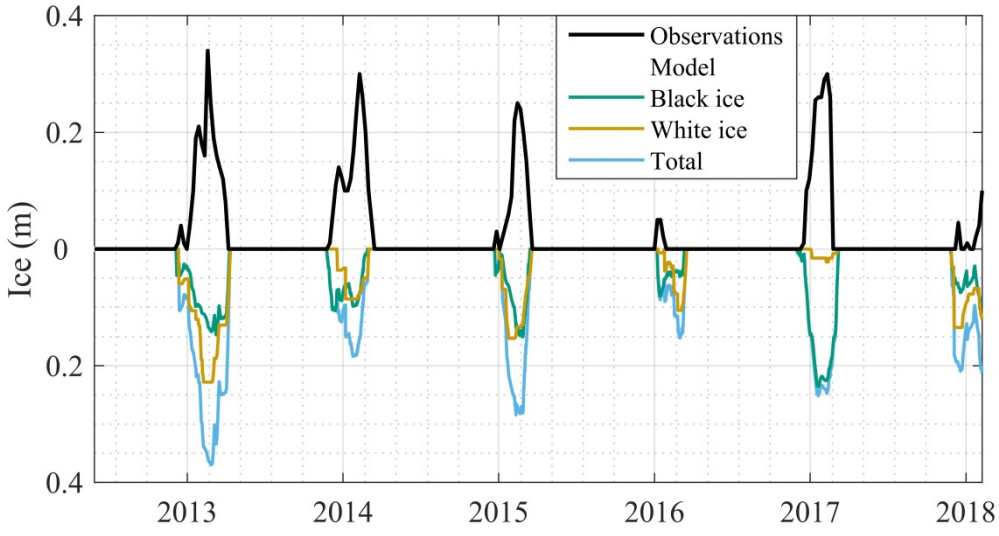

Figure B1. Ice model performance in Sihlsee (2012 to 2018) showing modelled white ice (orange), black ice (green) and total ice cover (white- and black ice combined, in blue) against measurements (black).

Geosci. Model Dev. Discuss., https://doi.org/10.5194/gmd-2018-336
Manuscript under review for journal Geosci. Model Dev.
Discussion started: 1 April 2019

C. Estimation of clear-sky solar radiation

The algorithm below is based on the equations from the Lake HeatFluxAnalyzer (see http://heatfluxanalyzer.gleon.org/), following the methods of Meyers and Dale (1983).

Declination of the sun [rad]: $\delta = \sin^{-1}(-0.39779 \cos\frac{2\pi \mathrm{DOY_s}}{365.24})$, where $\mathrm{DOY_s}$ is the day of year after the winter solstice (December 21st).

Cosine of the solar zenith angle [-]: $\cos Z = \max(\sin\varphi \sin\delta + \cos\varphi \cos\delta \cos\frac{\pi(\mathrm{H}-12.5)}{12}, 0)$, where φ is the latitude in radians and H is the hour of the day, assuming the solar noon is at 12h30.

Air mass thickness coefficient [-]: $m = 35 \cos Z\ (1244 \cos^2 Z + 1)^{-0.5}$

Dew point temperature [°C]: $T_d = 243.5 \log\frac{p_w}{6.112} / (17.67 - \log\frac{p_w}{6.112}) + 33.8$, where p_w[mbar] is the water vapour pressure.

Precipitable water vapour [cm]: $w_p = e^{0.1133 - \log(G+1) + 0.0393(1.8\,T_d + 32)}$, where G is an empirical constant dependent on latitude and day of year (see tables from Smith, 1966).

Attenuation coefficient for water vapour [-]: $\lambda_w = 1 - 0.077\ (w_p m)^{0.3}$

Attenuation coefficient for aerosols [-]: $\lambda_a = 0.935^m$

Attenuation coefficient for Rayleigh scattering and permanent gases [-]: $\lambda_{Rg} = 1.021 - 0.084(m\ (0.000949 p_a + 0.051))^{0.5}$, where p_a [mbar] is the air pressure.

Effective solar constant [W m^{-2}]: $I_{\mathrm{eff}} = 1353(1 + 0.034\cos\frac{2\pi \mathrm{DOY}}{365.24})$, where DOY is the day of year.

Clear-sky solar radiation [W m^{-2}]: $H_{\mathrm{cs}} = I_{\mathrm{eff}} \cdot \cos Z \cdot \lambda_w\ \lambda_a\ \lambda_{Rg}$